Pol. J. Environ. Stud. Vol. 31, No. 5 (2022), 4805-4816
DOI: *10.15244/pjoes/149412* ONLINE PUBLICATION DATE: 2022-08-08

Original Research

Spatial Distribution and Sources of Dissolved Organic Matter in High-Antimony Shallow Groundwater in the Xikuangshan Mine, Hunan, China

Yingao Peng[1,2], Chunming Hao[2]*, Hongbiao Gu[1]

[1]Institute of Disaster Prevention, Sanhe Hebei China, 065201
[2]North China Institute of Science and Technology, Sanhe Hebei China, 065201

Received: 4 February 2022
Accepted: 23 April 2022

Abstract

The origin and composition of dissolved organic matter (DOM) is crucial for fate of antimony (Sb) in aquatic systems. However, there are in which DOM compositional properties, that may better explain the biogeochemical process of Sb, have been absent. This study aimed to understand the fraction, spatial distribution, and spectral characteristics of DOM in high-Sb groundwater (commonly: >0.005 mg/L) from the Xikuangshan Mine in Lengshuijiang, Hunan, China, and explore the characteristics of DOM associated with the formation process of high-Sb groundwater. Inductively coupled mass spectrometry and excitation/emission matrix-parallel factor analysis were used to determine the Sb content, DOM composition, and fluorescence characteristics of 25 shallow groundwater samples collected in May 2021. The dissolved organic carbon (DOC) values in the shallow groundwater varied from 0.38±1.89 to 9.90±1.89 mg/L, with a mean of 2.49 mg/L. The DOM consisted of the following four components: C1, terrestrial humus; C2, microbial humus; C3, fulvic acid; and C4, tryptophan. DOM in high-Sb groundwater usually has a high humification index, low biological index, and low fluorescence intensity values. This result will help to understand the effect of DOM on the accumulation and migration of antimony in groundwater during biogeochemical cycling.

Keywords: Xikuangshan, high-antimony shallow groundwater, DOM, fluorescence index

Introduction

Antimony (Sb), a ubiquitous toxic metalloid, is one of the priority pollutants cited by the European Union and the United States [1] as causing serious environmental issues and harming the human immune system and nervous system, gene expression, and development [2]. The elevated levels of Sb in groundwater systems caused by increasing mine activities during the past decades have received considerable attention worldwide.

Groundwater is the most important source of drinking water globally and is consumed by approximately 1.5 billion people each day. Typical

*e-mail: haocm@ncist.edu.cn

concentrations of dissolved Sb in unpolluted groundwater are usually well below 0.001mg/L [3]. Hence, to improve the quality of groundwater used for drinking, most countries and health organizations have established drinking water quality guidelines for Sb; these values include 0.020 mg/L as set by the World Health Organization [3], 0.006 mg/L by the United States [4], 0.005 mg/L by the European [5] and China [6]. High-Sb groundwater (commonly: >0.005 mg/L) has been widely reported in mining areas globally, particularly in Slovakia [7], Scotland [8], Australia [9], Portugal [10], Egypt [11], Italy [12], Mexico [13], Luxembourg [14], China [15]. In China, high-Sb groundwater is distributed in the Hunan, Guangxi, Guizhou, Yunnan, and Tibet provinces [15]. This high-Sb groundwater is evident in the Xikuangshan (XKS) Mine in the Hunan Province, where the background Sb concentration is 0.015 mg/L [16].

Numerous scholars have conducted studies relating to Sb concentrations in groundwater. For example, Sb contamination has been previously evaluated in terms of pH [17], temperature [18], valance state, and Fe concentration [19-21]. Exposed stibnite is converted to Sb(III) oxide, which is further oxidized to Sb(V) and transferred to groundwater [22]. The source, migration, and transformation of Sb pollutions in groundwater have been traced by environmental isotopes such as those of S and Sr [23]. The effect of HA on Sb behavior during Fe(II)-induced ferrihydrite transformation has been previously examined [24]. Likewise, the effects of Fe(II) on the oxidation and adsorption of Sb(III) by MnO_2 under acidic conditions have also been examined [25]. Investigations regarding the formation mechanism of high-Sb groundwater have significantly advanced in recent years. Analysis of hydrogeochemical characteristics showed that the high Na^+, high total dissolved solids (TDS), and high SO_4^{2-} enrichment favored in high-Sb groundwater are primarily controlled by Ca-HCO_3-SO_4, followed by Ca-Na-SO_4 and Ca-SO_4-HCO_3 [16, 26]. The chemical composition of high-Sb groundwater is controlled by ion-exchange interactions and the dissolution of carbonate and silicate minerals, for which ion-exchange interaction is the most important factor [16, 26].

Dissolved organic matter (DOM) has been an issue of global focus, as it alters redox environments to generate high-As groundwater [27-29]. High-As groundwater in China is mainly distributed in Guizhou, Inner Mongolia, Shanxi, Taiwan, Yunnan, and Xinjiang [30]. Two typical high-As groundwater areas are the Hetao Basin, a typical sediment-filled basin in northwest China with groundwater DOC concentrations from 4.70 to 12.8 mg/L [31], and the Han River Plain with dissolved organic carbon (DOC) concentrations between 1.35 and 45.33 μg/L [32]. In recent years, it has become commonly accepted that the mechanism of As enrichment is the synergism of microorganisms and DOM catalyzing the reductive dissolution of As-adsorbing Fe/Mn oxide minerals and reducing adsorbed As(V) under reducing conditions [31]. Generally, the chemical properties of Sb are similar to those of As [33]. Nevertheless, the distribution of DOM in high-Sb groundwater is not well understood, and it is unknown whether it affects the environmental behavior of elemental Sb.

Approximately 80% of the annual global production of Sb comes from China, of which 70% comes from XKS mines in the Hunan Province [34]. The XKS Sb mine is nicknamed the "World's Antimony Capital" because it has abundant Sb resources, produces the most Sb in the world, and has high-grade Sb [35]. However, over 120 years of Sb mining has caused a series of environmental problems there, such as ground collapse, aquifer dewatering, land resource destruction, and water contamination [23]. The Magunao and Shetianqiao aquifers are major drinking aquifers that have become contaminated with Sb from a massive open pile of waste rock, smelting slag, and tailings. In recent research, Sb concentrations in the surface water around the XKS mine were reported to be 4581-29423 μg/L [36]. Sb concentrations up to 1.5-3799.4 mg/kg were detected in near-surface soils at the XKS mine [37]. The average Sb concentration of local groundwater was 27.4 μg/L [38]. Furthermore, the Sb concentrations in terrestrial and aquatic invertebrates and amphibians in the XKS mine area were 30400 μg/kg, 5200 μg/kg, and 2300 μg/kg [35], respectively.

Hence, the objectives of this study were as follows: (1) investigate the high-Sb shallow groundwater DOM content and spatial distribution in the XKS region of Hunan, China; (2) analyze the sources of high-Sb shallow groundwater DOM; and (3) explore the mechanism by which DOM elevates the concentration of soluble Sb in high-Sb shallow groundwater. This study provides a good understanding of the formation of high-Sb groundwater and the role of DOM in the formation mechanisms of high-Sb groundwater.

Study Area

The largest Sb mine in the world is the XKS Sb mine, located in Lengshuijiang, Hunan, China, at 27°46-27°49 N and 111°28-111°32 E (Fig. 1). It covers an area of approximately 26 km^2 and is at an altitude of 220-823.2 m (low hilly topography). The Sb mine area consists of southern and northern mines, with a retained resource reserve of 400,000 tons of Sb, and production by the largest Sb producing company (Hsikang Shan Twinkling Star) in the XKS mine area reaching 5.5 tons per year. The XKS mine area is characterized by a subtropical monsoon climate, and the average annual temperature, precipitation, and evaporation are 16.7ºC, 1381.60 mm, and 903.30 mm, respectively. The Qingfeng, Batangshan, and Tanjia rivers flow through the study area before they merge into the Zijiang River, which eventually drains into the Yangtze River.

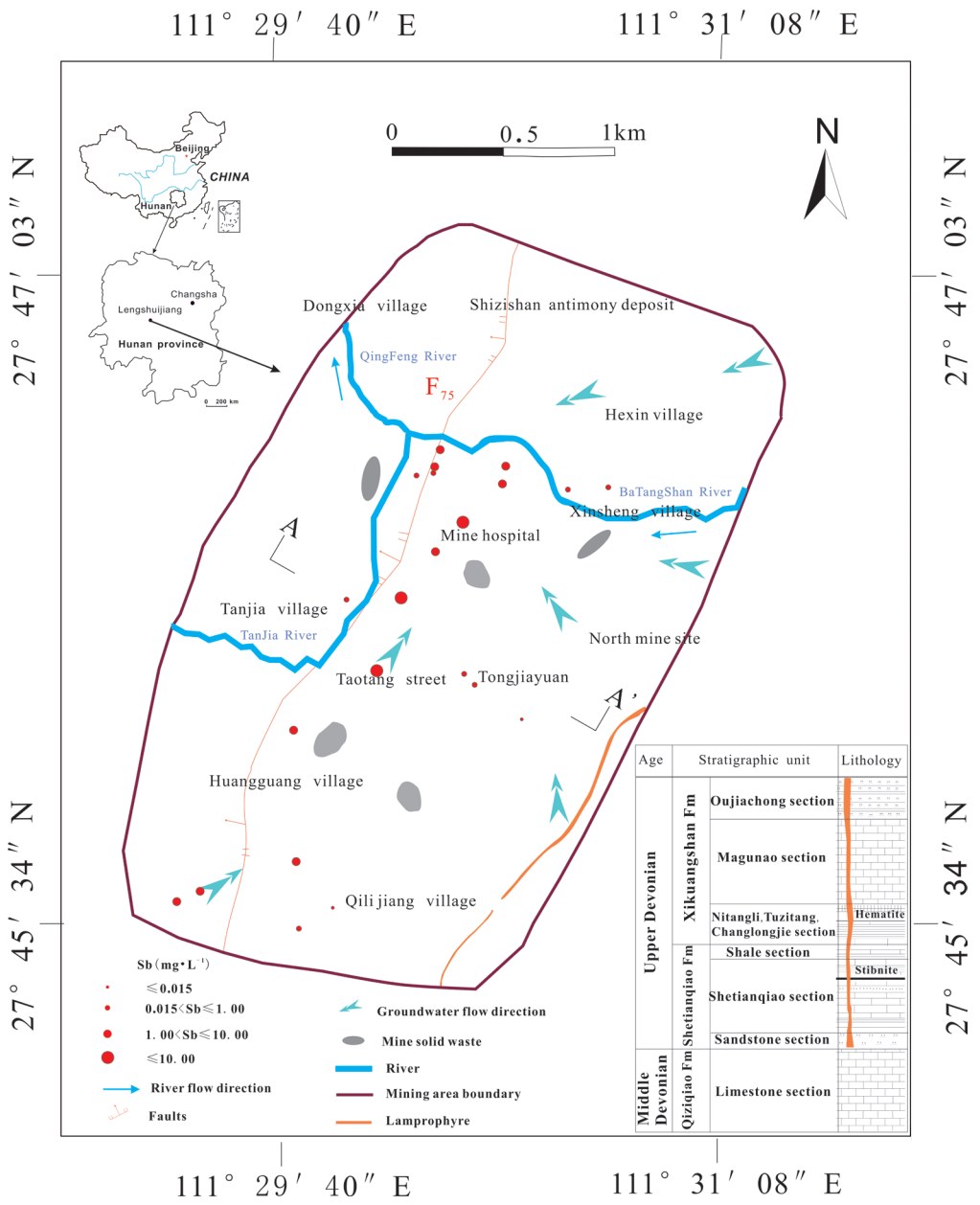

Fig. 1. Geological map of the Xikuangshan mine showing groundwater sampling sites.

The main aquifers within the XKS mine area are the Magunao (MA) and Shetianqiao (SA) aquifers (Fig. 2), with lithologies of micrite and clip sandy limestone, siltstone, mudstone, and shale, respectively. Due to the lack of karst development, the aquifuge between the MA and SA aquifers has a weak water yield property. The two major aquifers are widely spaced and have weak hydraulic connections. The deposit of the XKS mine area is controlled by NE–SW trending main F_{75} faults and a lamprophyre vein (Fig. 1). The SA aquifer contains 13 layers of stibnite, which is the main mining horizon at the mine.

The MA aquifer is a heavily exposed carbonate karst fracture aquifer that is 258 m thick. It is recharged by the infiltration of atmospheric precipitation and discharges mainly into springs, and rarely by fault drainage. The shallowness of the groundwater makes this aquifer an essential source of drinking water for 9000 local residents. The chemical composition of unpolluted shallow drinkable groundwater is Ca-HCO_3-SO_4. The MA aquifer was covered by a large amount of solid mine waste such as waste rocks and slag (Fig. 1).

Material and Methods

Sample Collection and Preservation

Sampling was carried out in May 2021, and 25 shallow groundwater samples were collected from the study area as shown in Fig. 1. Groundwater sampling

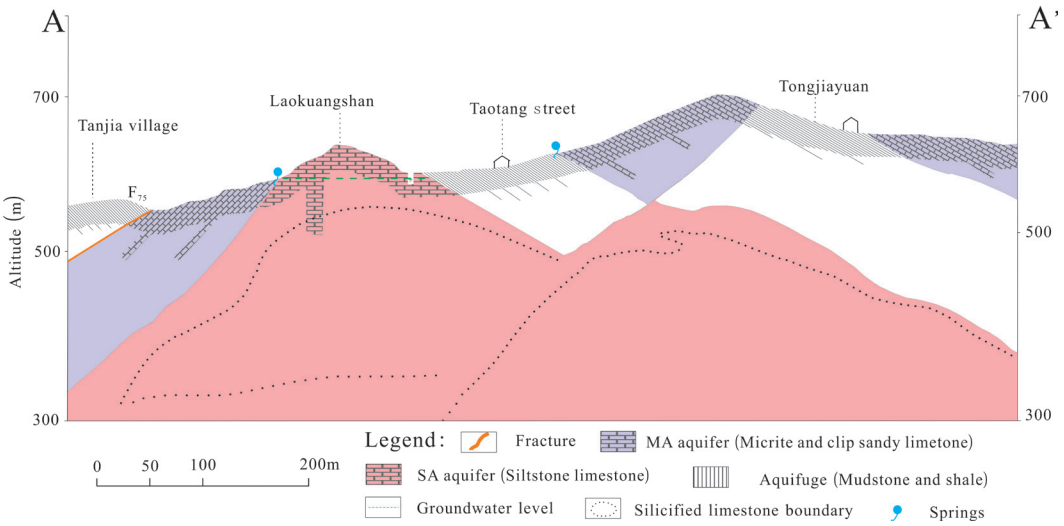

Fig. 2.Stratigraphic section of the Xikuangshan mine.

sites were employed based on the landform and representative springs of the sampling area. The limit value of antimony in the Chinese National Water Quality Sanitation Standards is 0.005 mg/L, however, the environmental background value of antimony in study area reaches 0.015 mg/L. To facilitate the study of high-Sb groundwater (comparison with previous studies: [16] [23]), it was divided into four groups according to its Sb concentration: low-Sb groundwater (Class I: Sb≤0.015 mg/L), relatively high-Sb groundwater (Class II: 0.015<Sb≤1.00 mg/L), ultra-high-Sb groundwater (Class III: 1.00<Sb≤10.00 mg/L), and extremely high-Sb groundwater (Class IV: Sb>10.00 mg/ L), where class II, III and IV groundwater are collectively referred to as high-Sb groundwater.

Geographical coordinates were obtained at each sampling site using a handheld GPS device (GPSMAP 63csx, Garmin, USA). Physicochemical parameters such as pH, temperature, electrical conductivity, redox potential, and TDS were measured in the field using a portable multiparameter device (Aqua TROLL600, Vusitu, USA) that was calibrated daily. All equipment that came in contact with the water sample was washed three times therewith prior to the measurements. Before collection, every polyethylene bottle used in the sampling was washed 2-3 times with distilled water and again 2-3 times with a water sample. In addition, all the groundwater samples were fresh water. Following this, the water samples were filtered using 0.45 μm glass fiber membranes and collected in three replicates from each site; three bottles of 50 ml, 550 ml, and 550 mL water were collected. Amber bottles of 50 mL were used for DOM analysis, and all samples were stored in a refrigerator at 4ºC until laboratory analysis. To prevent Sb precipitation and for trace element analysis, 5 mL of 10% thiourea + 10% ascorbic acid mixed solution and 1:1 (V:V) nitric acid (until pH<2) were added to the first 550 mL bottles of water samples. The final 550 mL bottles were used to measure Sb accurately; 1.00 mol/L Sb standard solution was mixed into every sampling bottle, which was then shaken well. As soon as possible after sample collection, and no later than three days, samples were transported to the laboratory for processing.

Sample Analysis

DOC concentrations were measured by wet oxidation using a total organic carbon analyzer (TOC-5000, Shimadzu, Japan) with an analysis precision of 0.01 mg/L [27]. The Sb concentration of each water sample was measured using an Agilent 7700x inductively coupled mass spectrometer with indium as the internal standard [23]. The precision of the Sb element analysis was 0.001 mg/L and the precision of the pH analysis was set at 0.1.

Fluorescence and Parallel Factor (PARAFAC) Modeling

Prior to spectroscopic analysis, the temperatures of the refrigerated water samples were warmed to room temperature. Fluorescent excitation/emission matrix (EEM) spectra were obtained in 2 nm and 1 nm increments, respectively, using a Hitachi F-4600 spectrofluorometer with an excitation range of 250-600 nm and an emission range of 300-600 nm. The scan integration time was 0.1 s and the scan speed was 3200 nm/s. Milli-Q ultrapure water (18.2 MΩ/cm) blanks were analyzed using Rayleigh scattering and Raman peaks were obtained from sample EEMs, after which Raman normalization was conducted using the Raman peak of ultrapure water. The intensity of the fluorescent component was expressed in units of R.U [29].

Following the techniques used by other researchers, the fluorescent components of calibrated EEMs were modeled using parallel factor (PARAFAC) analysis

performed in MATLAB2017b with the DOMFluor toolbox [39], and the residual scattering peak of the fluorescence spectrum was removed using the drEEM toolbox [39]. The number of fluorescent components was determined using minimum residual analysis, and the reliability of the results was discussed using a half-analysis.

Analytical Quality Control

To ensure the precision and accuracy of the analytical results, 10% of the samples submitted for analysis were blind samples, and the chemical analysis of each water sample was performed in triplicate. Valid data are the average values of the three tests, which have a maximum sub-10% relative standard deviation. Recovery rates of over 95% for Sb were determined by spiking the water samples with a standard Sb solution. The DOC concentration errors of these water samples were all below 5%. Moreover, 20% of the water samples were analyzed. The errors between the outcomes of the duplicate samples were equal to or less than 10%.

Results and Discussion

Hydrochemical Analysis

The descriptive statistics for the indicators analyzed in the groundwater samples in the XKS mine area are summarized in Table 1. The pH of the shallow groundwater ranged from 4.97±0.77-9.36±0.77, with a mean of 7.14. In addition, the pH values for 84% of the sampling points met China's national drinking water quality guidelines (6.5-8.5) (GB5749-2006). According to previous reports [16, 23], the shallow groundwater in the area is mainly weakly alkaline. The concentrations of Sb were 0.001±5.557-18.402±5.557 mg/L, with mean values of 3.407 mg/L. The highest Sb content in shallow groundwater was 1226 times the maximum acceptable Sb concentration (0.015 mg/L) according to the guidelines. This result is similar to that of previous research, where the Sb content of dispersed drinking water from XKS Sb mines reached 0.015-4.74 mg/L, with a mean value of 4.557 mg/L [23]; the Sb content in high-Sb shallow groundwater reached 0.024±0.001-9.810±0.001 mg/L, with a mean value of 1.577 mg/L [16] . The TDS values of high-Sb shallow groundwater samples ranged from 135±320 to 1229±320 mg/L. In addition, 8% of high-Sb shallow groundwater samples have TDS values above 1000 mg/L, which exceeds this guideline (GB5749-2006).

Concentration of Dissolved Organic Carbon in Shallow Groundwater

DOC can be used as an alternative measure of DOM in groundwater [40]. The DOC values in shallow groundwater vary from 0.38±1.89 to 9.90±1.89 mg/L (Table 1), with a mean of 2.49 mg/L. Statistically, DOC values in the range of 1.00-3.00 mg/L accounted for 89.40% of the study area, with concentrations below 1.00 mg/L accounting for a minimum of 0.35%, and concentrations of 3.00-5.00 mg/L, 5.00-7.00 mg/L, and >7.00 mg/L accounting for 8.66%, 1.11%, and 0.49%, respectively (Fig. 3). The spatially high DOC values in the study area are in the central area of the mine (Fig. 3), similar to the distribution of high-Sb groundwater, which implies that DOM plays an important role in the formation of high-Sb groundwater.

Characterization of the Fluorescence Components of Dissolved Organic Matter (DOM)

A PARAFAC model was used to decompose the EEM dataset of the 25 high-Sb shallow groundwater samples identified four different DOM components (Fig. 4). Furthermore, comparison with the fluorescence peaks characteristic of DOM components from previous studies (Table 2) showed that components C1, C2, and C3 are all humic-like fluorescent components, with the difference that C1 (340/450 nm) corresponds to the traditional C peak and represents a humic component of terrestrial origin, which can persist consistently [41]. C2 (320/400 nm) corresponds to the traditional M peak and represents a microbial humic-like component with a low molecular weight, typically produced by the degradation of other humic substances [42]. C3 (350/520) is a fulvic acid-like substance [43] and C4 (290/340 nm) is a typical fluorescent protein-like component with excitation/emission wavelengths consistent with those of tryptophan (270-290/320-350 nm), indicating that C4 is mainly a tryptophan-like component [44]. Tyrosine (225, 275/300 nm), a protein-like components, were not observed in this study [44].

Table 1. Data for high-Sb shallow groundwater samples collected in this study.

Samples	Index	pH	Sb	TDS	DOC	FI	HIX	BIX
			mg/L					
25	Min	4.97	0.001	135	0.38	0.20	0.65	0.29
	Max	9.32	18.402	1229	9.90	1.83	10.71	1.73
	Ave	7.14	3.407	475	2.49	1.36	2.69	0.91
	SD	0.77	5.557	320	1.89	0.34	2.27	0.27

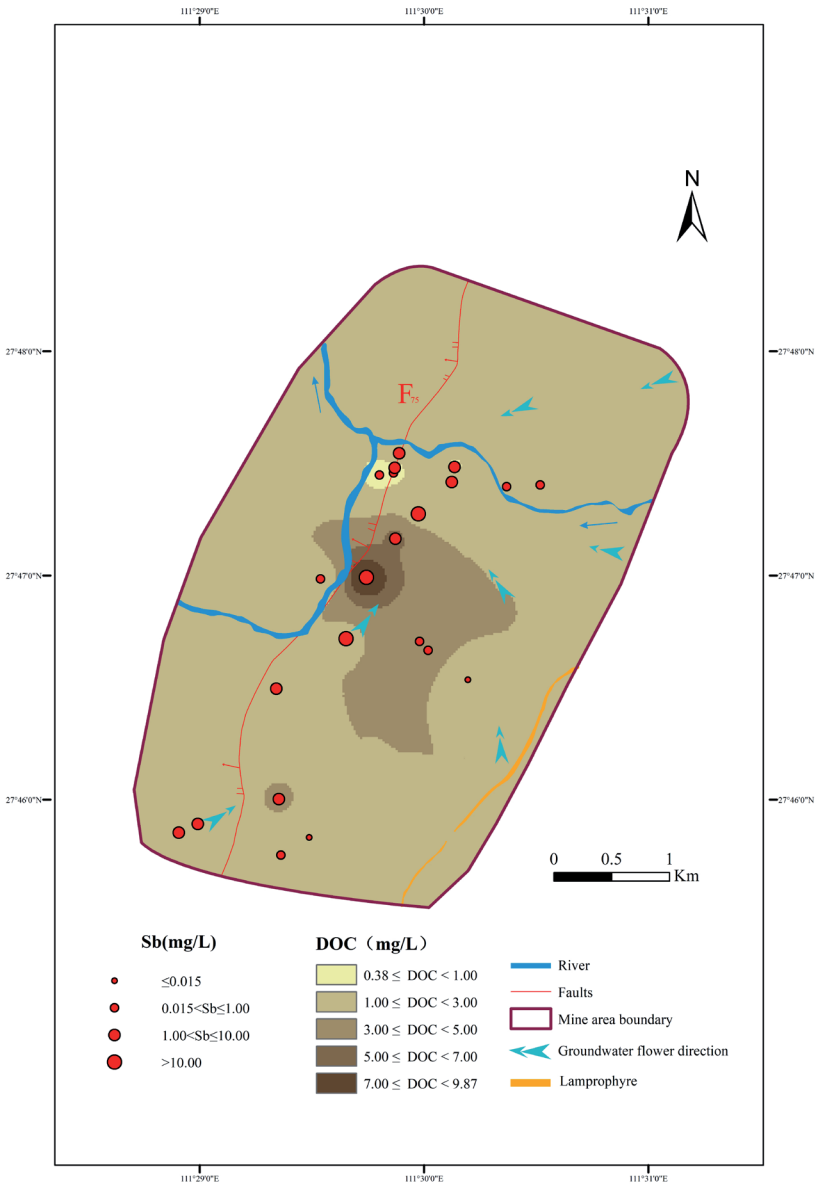

Fig. 3. Spatial distribution of dissolved organic carbon in high-antimony shallow groundwater in the Xikuangshan mine.

The percentages of the fluorescent components (C1, C2, C3, and C4) in the different Sb classes are summarized in Fig. 5. Although the percentages of the four fluorescent components demonstrated no significant differences among the four Sb classes, there were differences in the four fluorescent components themselves, for each Sb class. Using Class IV as an example, the percentages of C1 were 40.6±4.4%, which were 2.04-, 1.60-, and 2.87-fold higher than C2, C3, and C4, respectively. Overall, the highest relative contribution to the total fluorescence intensity of the samples came from the terrestrial humic-like substance C1, followed by the fulvic acid C3 and the microbial humic-like substance C2, with the lowest

Table 2. Spectral characteristics of the excitation/emission matrix of three fluorescent components.

Component	(Ex/Em)/nm	Probable origin	References: (Ex/Em)/nm
C1	340/450	Terrestrial humic	C2: 260(380)/480 [41]
C2	320/400	Microbial humic	SW2: 250(320)/407 [42]
C3	350/520	Humic like	390/509 [43]
C4	290/340	Protein-like	G6: 290/352 [44]

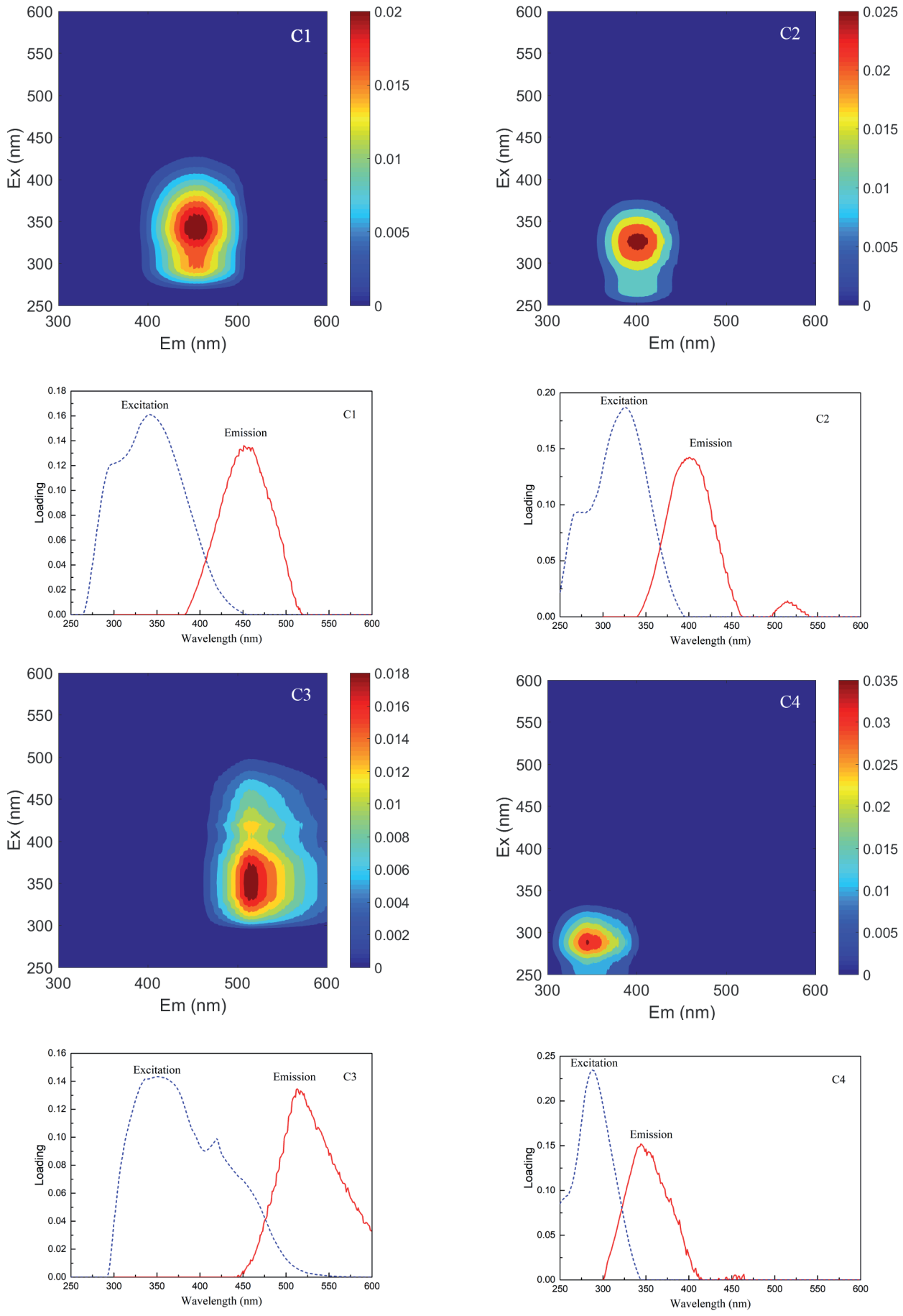

Fig. 4. Spectral characteristics of the four-component model identified using excitation/emission matrix-parallel factor analysis.

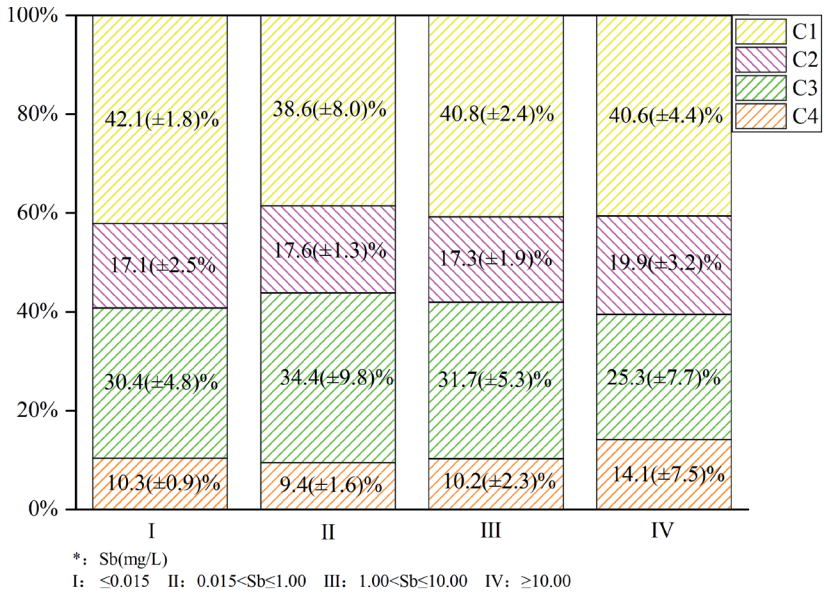

Fig. 5. Percentages of the components of dissolved organic matter in antimony-bearing groundwater.

relative contribution made by the tryptophan-like C4. The dominance of the C1 content makes the DOM source characteristics in groundwater biased toward terrestrial sources.

Optical DOM Indices

The DOM sources are primarily terrestrial or biogenic, and because fluorescence parameters are good indicators of the DOM source they are used to further analyze the spectral characteristics and sources of DOM in water bodies under different environmental influences. The fluorescence index (FI) is an indicator of DOM source, where FI<1.4 means that the DOM is derived mainly from terrestrial or soil input, FI>1.9 means that it comes mainly from autochthonous sources, and 1.4<FI<1.9 indicates that it is affected by both terrestrial and autochthonous sources. The biological index (BIX) and the humification index (HIX) were cited to further clarify the DOM source. When BIX>1, autochthonous source characteristics are strong and DOM is produced mainly by biological bacteria. Conversely, when BIX<1, anthropogenic or terrestrial source characteristics are strong. The HIX is used mainly to characterize the degree of humification of humic-like substances produced by terrestrial DOM sources. When HIX >16, it indicates a strong humic character and strong contribution from terrestrial sources; when HIX<4, DOM was characterized as having a biological or aquatic bacterial origin; when 4<HIX<6, it had a weak humic character; and 6<HIX<10 indicates an important humic character [45-50].

FI, BIX, and HIX values were 0.20±0.34-1.83±0.34, 0.29±0.27-1.73±0.27, and 0.65±2.27-10.71±2.27, respectively (Table 1), with mean values of 1.36, 0.91, and 2.69, respectively. Class IV groundwater had relatively lower BIX and FI and higher HIX than Class III, II, and I groundwater (Fig. 6, Fig. 7), indicating that DOM in Class IV groundwater a strong humic character and few autochthonous components. Class III and II groundwater have a significant tendency toward high HIX values and low BIX values, in contrast to Class I groundwater which is characterized by low humification and high biochemical properties. DOM in high-Sb groundwater and DOM in high-As groundwater may have similarities, with DOM in high-As groundwater [27] typically having higher HIX and lower BIX values and being more unsaturated, more humic, and less biodegradable.

As shown in Fig. 3, the spatial distribution of Class IV groundwater at the center of the mine area has high HIX and lower BIX and FI values, while Class III

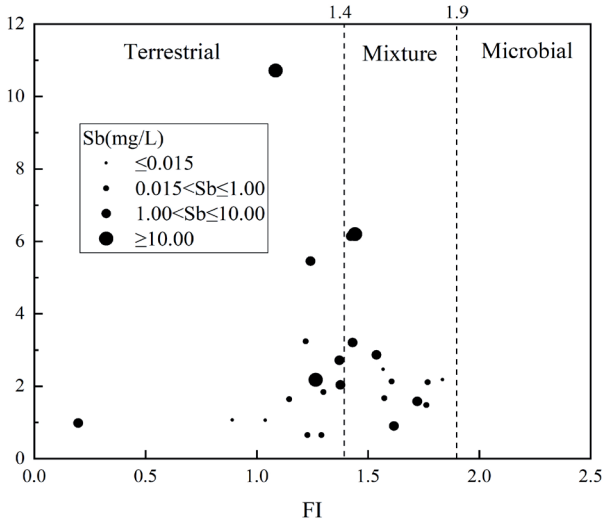

Fig. 6. Relationship between the humification index (HIX) and fluorescence index (FI) values of high-antimony shallow groundwater.

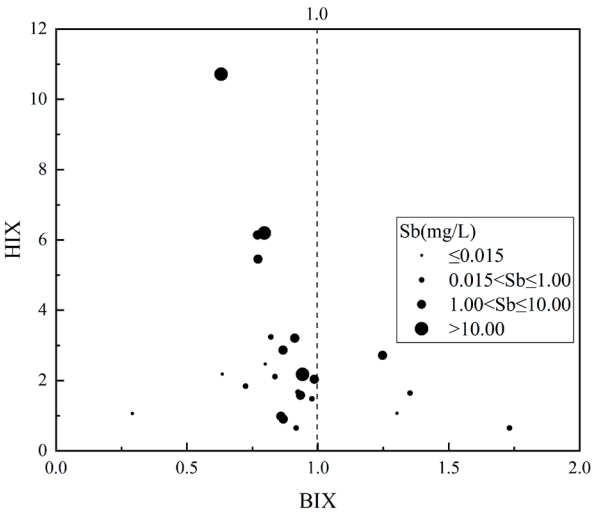

Fig. 7. Relationship between the humification index (HIX) and biological index (BIX) values of high-antimony shallow groundwater.

groundwater and Class II groundwater near the center of the mine area have lower HIX and higher BIX and FI values, comparatively. The BIX and FI of Class I groundwater away from the center of the mine are significantly higher than those of high-Sb groundwater, while the HIX is lower than that of high-Sb groundwater (Fig. 8b, c, d).

Analysis of the combined FI, BIX, and HIX values shows the source of DOM in the center of the mine is largely input from terrestrial sources, whereas the source of DOM in the area 1 km from the center of the mine is the result of a combination of terrestrial and autochthonous sources; the area away from the center of the mine is dominated by autochthonous sources. This difference may be due to the low vegetation cover in the center of the mine, where human and industrial activities are more intense, resulting in low bioavailability of DOM and thus low BIX values, while the long-term presence of terrestrial sources of humic substances results in high HIX values. This may

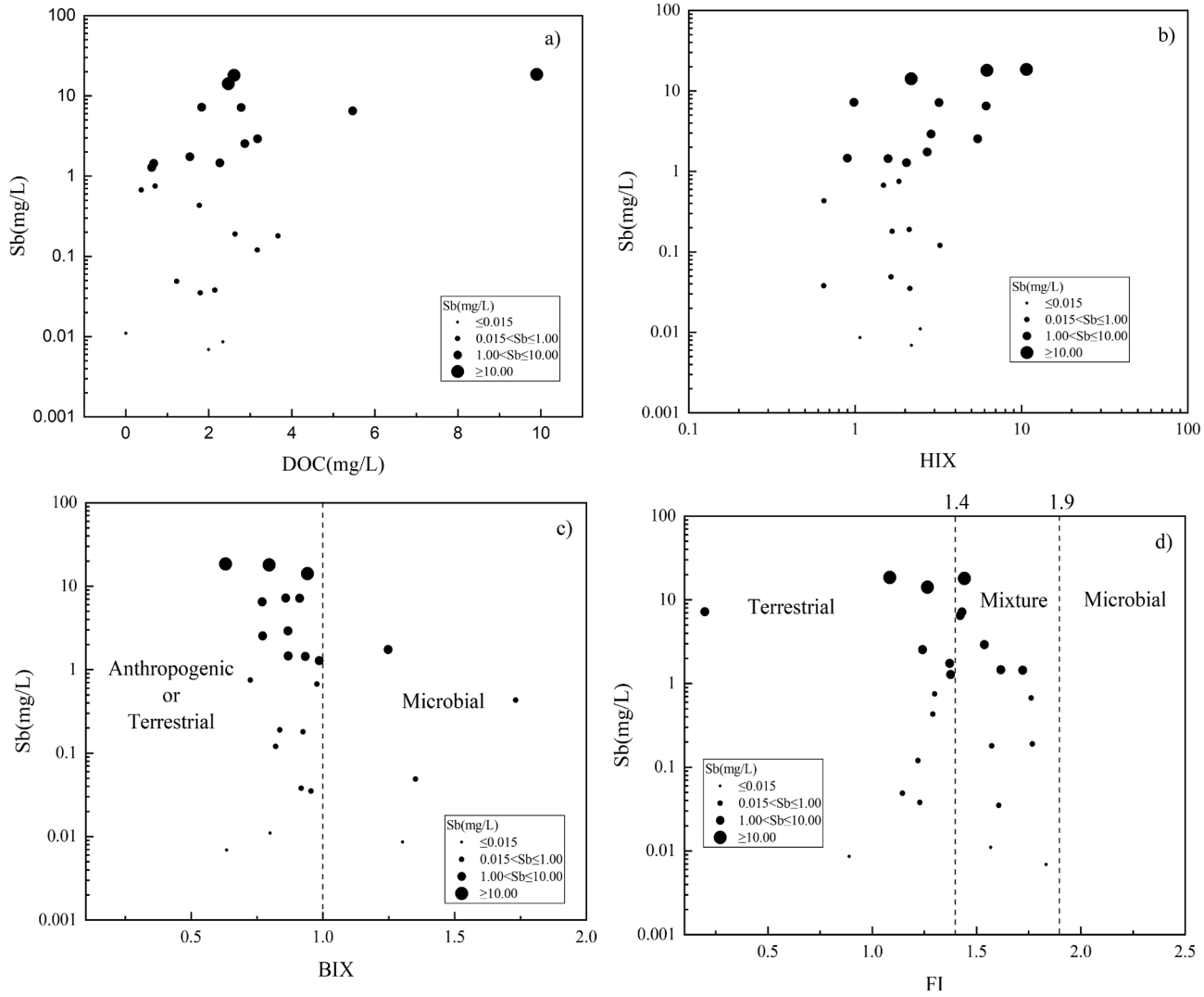

Fig. 8. Relationship between dissolved organic carbon (DOC) a), the humification index (HIX) b), the biological index (BIX) c), and fluorescence index (FI) d) and antimony values in high-antimony in shallow groundwater

have increased the number of autochthonous sources, resulting in a lower HIX. In addition, the humification of organic matter is influenced by the ambient redox potential, with both high and low potentials being detrimental to the humification of organic matter, resulting in a low HIX index [51].

Correlation between DOM and Sb Concentrations

The concentration distribution of total Sb tended to change from Class I to Class IV as the DOC content increased (Fig. 8a). The greater the HIX value, the trend from Class I to Class IV (Fig. 8b), while the smaller the BIX and FI values, the trend from Class I to Class IV (Fig. 8c, Fig. 8d). This indicates that low-Sb groundwater is characterized by low humification and high biodegradability. High-Sb groundwater has a comparatively higher HIX and lower BIX value, is less saturated, more humic, and less biodegradable.

Our study provides the distribution sources evidence that groundwater Sb concentrations and DOM compounds were positively correlated, which is similar with As studies [29-32]. These components of DOM may contribute to Sb accumulation and migration via electron shuttling, complexation, and competition for adsorption. Electron shuttling may directly or indirectly affect Sb oxides. During biogeochemical cycling, direct evidence that electron shuttling of DOM between Geobacter metal-lireducens and Fe (III) oxides in the Bay of Bengal Delta [52]. The concentrations of Sb in the environments are typically induced by Fe(oxy)(hydr)oxides [25]. Humic acid promoted the formation of substantial amounts of colloidal Sb during Fe (II)-induced ferrihydrite transformation [24].

Conclusion

In this study, the DOM content in high-Sb shallow groundwater in XKS mine area, and the spatial distribution and spectral characteristics were investigated using EEMs, and fluorescence indices to determine the close relationship between DOM and high-Sb shallow groundwater in the XKS mine area. We found that DOM extracted from the groundwater of XKS area was mainly derived from the mixture of terrestrial and autogenous sources. Moreover, the values of DOC in shallow groundwater vary from 0.38±1.89 to 9.90±1.89 mg/L, with a mean of 2.49 mg/L, similar to the distribution of high-Sb groundwater. Components of DOM may contribute to Sb accumulation and migration via electron shuttling, complexation, and competition for adsorption. This result will help to understand the effect of DOM on the accumulation and migration of antimony in groundwater during biogeochemical cycling. However, we did not establish comparative experiments to quantitatively confirm whether the enrichment and migration of Sb in groundwater is dominated by DOM, which will be the topic of further research.

Acknowledgments

This work was supported by the Natural Science Foundation of Hebei Province (D2021508004); the ecological restoration project in the Lengshuijiang antimony mine area (grant LCG2020009).

Conflict of Interest

The authors declare no conflict of interest.

References

1. FANG L., ZHOU A., LI X., ZHOU J., PAN G., HE N. Response of antimony and arsenic in karst aquifers and groundwater geochemistry to the influence of mine activities at the world's largest antimony mine, central China. Journal of Hydrology, **603** (C), 127131, **2021**.
2. BOREIKO C.J., ROSSMAN T.G. Antimony and its compounds: Health impacts related to pulmonary toxicity, cancer, and genotoxicity. Toxicology and Applied Pharmacology, **403**, 115156, **2020**.
3. WHO. Guidelines for Drinking-water Quality, fourth ed.; World Health Organization, 314, **2017**.
4. EPA. Implementation Guidance for the Arsenic Rule. U.S. Government Printing Office. EPA report-816-D-02-005, **2002**.
5. Council of the European Communities. Council Directive 76/464/EEC of 4 May 1976 on pollution caused by certain dangerous substances discharged into the aquatic environment of the Community. Official Journal L 129, 18/05/1976, 23, **1976**.
6. MHPRC. Standards for Drinking Water Quality. Ministry of Health P.R.China, GB 5749, **2006**.
7. JURKOVIČ L., MAJZLAN J., HILLER E., KLIMKO T., VOLEKOVÁ-LALINSKÁ B., MÉRES Š., GÖTTLICHER J., STEININGER R. Natural attenuation of antimony and arsenic in soils at the abandoned Sb-deposit Poproč, Slovakia. Environ Earth Sci, **78**, 672, **2019**.
8. MACGREGOR K., MACKINNON G., FARMER J.G., GRAHAMA M.C. Mobility of antimony, arsenic and lead at a former antimony mine, Glendinning, Scotland. Science of The Total Environment, **529**, 213, **2015**.
9. WARNKEN J., OHLSSON R., WELSH D.T., TEASDALE P.R., CHELSKY A., BENNETT W.W. Antimony and arsenic exhibit contrasting spatial distributions in the sediment and vegetation of a contaminated wetland. Chemosphere, **180**, 388, **2017**.
10. NEIVA A.M., ANDRŠ P., RAMOS J.M. Antimony quartz and antimony-gold quartz veins from northern Portugal. Ore Geology Reviews, **34** (4), 533, **2008**.
11. EL-BADRY A.E-M., KHALIFA M.M. The occurrence and distribution of high-arsenic, selenium, tin and antimony in bottom sediments of Burullus lagoon and its effects on human health, Egypt. Journal of African Earth Sciences, **136**, 305, **2017**.

12. CIDU R., BIDDAU R., DORE E., VACCA A., MARINI L. Antimony in the soil-water-plant system at the Su Suergiu abandoned mine (Sardinia, Italy): Strategies to mitigate contamination. Science of The Total Environment, **497-498**, 319, **2014**.
13. OSUNA-MARTÍNEZ C.C., ARMIENTA M.A., BERGÉS-TIZNADO M.E., PÁEZ-OSUNA F. Arsenic in waters, soils, sediments, and biota from Mexico: An environmental review. Science of The Total Environment, **752**, 142062, **2021**.
14. GESELS J., DOLLÉ F., LECLERCQ J., JURADO A., BROUYÈRE S. Groundwater quality changes in peri-urban areas of the Walloon region of Belgium. Journal of Contaminant Hydrology, **240**, 103780, **2021**.
15. HE M., WANG X., WU F., FU Z. Antimony pollution in China. Science of The Total Environment, **421-422**, 41, **2012**.
16. HAO C., ZHANG W., GUI H. Hydrogeochemistry characteristic contrasts between low- and high-antimony in shallow drinkable groundwater at the largest antimony mine in hunan province, China. Applied Geochemistry, **117**, 104584, **2020**.
17. HU X., GUO X., HE M., LI S. pH-dependent release characteristics of antimony and arsenic from typical antimony-bearing ores. Journal of Environmental Sciences, **44**, 171, **2016**.
18. HU X., HE M., LI S. Antimony leaching release from brake pads: Effect of pH, temperature and organic acids. Journal of Environmental Sciences, **29**, 11, **2015**.
19. GUO W., FU Z., WANG H., SONG F., WU F., GIESY J.P. Environmental geochemical and spatial/temporal behavior of total and speciation of antimony in typical contaminated aquatic environment from Xikuangshan, China. Microchemical Journal, **137**, 181, **2018**.
20. GUO X., WU Z., HE M., MENG X., JIN X., QIU N., ZHANG J. Adsorption of antimony onto iron oxyhydroxides: Adsorption behavior and surface structure. Journal of Hazardous Materials, **276**, 339, **2014**.
21. KONG L., HE M., HU X. Rapid photooxidation of Sb(III) in the presence of different Fe(III) species. Geochimica et Cosmochimica Acta, **180**, 214, **2016**.
22. ASHLEY P.M., CRAW D., GRAHAM B.P., CHAPPELL D.A. Environmental mobility of antimony around mesothermal stibnite deposits, New South Wales, Australia and southern New Zealand. Journal of Geochemical Exploration, **77** (1), 1, **2003**.
23. WEN B., ZHOU J., ZHOU A., LIU C., XIE L. Sources, migration and transformation of antimony contamination in the water environment of Xikuangshan, China: Evidence from geochemical and stable isotope (S, Sr) signatures. The Science of the total environment, **569-570**, 114, **2016**.
24. KARIMIAN N., BURTON E.D., JOHNSTON S.G., HOCKMANN K., CHOPPALA G. Humic acid impacts antimony partitioning and speciation during iron(II)-induced ferrihydrite transformation. Science of The Total Environment, **683**, 399, **2019**.
25. ZHANG C., HE M., OUYANG W., LIN C., LIU X. Influence of Fe(II) on Sb(III) oxidation and adsorption by MnO_2 under acidic conditions. Science of The Total Environment, **724**, 138209, **2020**.
26. LI C., HAO C., ZHANG W., GUI H. High Antimony Source and Geochemical Behaviorsin Mine Drainage Water in China's Largest Antimony Mine. Polish Journal of Environmental Studies, **29** (5), 3663, **2020**.
27. QIAO W., GUO H., HE C., SHI Q., ZHAO B. Unraveling roles of dissolved organic matter in high arsenic groundwater based on molecular and optical signatures. Journal of Hazardous Materials, **406**, 124702, **2021**.
28. ADELEH A., JŐRG R., SABRY M.S., NABEEL K.N., EDUARDO M., JŐRG S., KLAUS-HOLGER K. Review on the interactions of arsenic, iron (oxy)(hydr)oxides, and dissolved organic matter in soils, sediments, and groundwater in a ternary system. Chemosphere, **286** (2), 131790, **2021**.
29. HARSHAD K., NATALIE M., DATTA S. Effects of acidification on the optical properties of dissolved organic matter from high and low arsenic groundwater and surface water. Science of the Total Environment, **653**, 1326, **2019**.
30. GUO H., WEN D., LIU Z., JIA Y., GUO Q. A review of high arsenic groundwater in Mainland and Taiwan, China: Distribution, characteristics and geochemical processes. Applied Geochemistry, **41**, 196, **2014**.
31. LI X., GUO H., ZHENG H., XIU W., HE W., DING Q. Roles of different molecular weights of dissolved organic matter in arsenic enrichment in groundwater: Evidences from ultrafiltration and EEM-PARAFAC. Applied Geochemistry, **104**, 124, **2019**.
32. YU K., DUAN Y., GAN Y., ZHANG Y., ZHAO K. Anthropogenic influences on dissolved organic matter transport in high arsenic groundwater: Insights from stable carbon isotope analysis and electrospray ionization Fourier transform ion cyclotron resonance mass spectrometry. The Science of the total environment, **708**, 135162, **2020**.
33. WILSON N.J., CRAW D., HUNTER K. Antimony distribution and environmental mobility at an historic antimony smelter site, New Zealand. Environmental pollution, **129** (2), 257, **2004**.
34. DUPONT D., ARNOUT S., JONES, P.T., BINNEMANS K. Antimony recovery from end-of-life products and industrial process residues: a critical review. Green Chem. **2** (1), 79, **2016**.
35. FU Z., WU F., AMARASIRIWARDENA D., MO C., LIU B., ZHU J., DENG Q., LIAO H. Antimony, arsenic and mercury in the aquatic environment and fish in a large antimony mining area in Hunan, China. Science of The Total Environment, **408** (16), 3403, **2010**.
36. ZHU J., WU F., DENG Q., SHAO S., MO C., PAN W., LI W., ZHANG R. Environment characteristics of water near the Xikuangshan antimony mine, Hunan Province. Acta Scientiae Circumstantiate, **29** (03), 655, **2009** [In Chinese].
37. LI X., YANG H., ZHANG C., ZENG G., LIU Y., XU W., WU Y., LAN S. Spatial distribution and transport characteristics of heavy metals around an antimony mine area in central China. Chemosphere, **170**, 17, **2017**.
38. FU Z., WU F., MO C., DENG Q., MENG W., GIESY J.P. Comparison of arsenic and antimony biogeochemical behavior in water, soil and tailings from Xikuangshan, China. Science of The Total Environment, **539**, 97, **2016**.
39. QIAN C., WANG L., CHEN W., WANG Y., LIU X., JIANG H., YU H. Fluorescence Approach for the Determination of Fluorescent Dissolved Organic Matter. Analytical Chemistry, **89** (7), 4264, **2017**.
40. REN H., MA F., YAO X., SHAO K., YANG L. Multi-spectroscopic investigation on the spatial distribution and copper binding ability of sediment dissolved organic matter in Nansi Lake, China. Journal of Hydrology, **591** (125289), **2020**.
41. XU X., KANG J., SHEN J., ZHAO S., WANG B., ZHANG X., CHEN Z. EEM–PARAFAC characterization

of dissolved organic matter and its relationship with disinfection by-products formation potential in drinking water sources of northeastern China. Science of The Total Environment, **774**, 145297, **2021**.
42. PITTA E., ZERI C. The impact of combining data sets of fluorescence excitation - emission matrices of dissolved organic matter from various aquatic sources on the information retrieved by PARAFAC modeling. Spectrochimica Acta Part A: Molecular and Biomolecular Spectroscopy, **258**, 119800,**2021**.
43. CHARLES H.L., SAAVEDRA S.S. Conformational changes in a soil fulvic acid measured by time-dependent fluorescence depolarization. Analytical chemistry, **58**, 1978, **1986**.
44. MURPHY K.R., HAMBLY A., SINGH S., HENDERSON R. K., BAKER A., STUETZ R., KHAN S.J. Organic matter fluorescence in municipal water recycling schemes: toward a unified PARAFAC model. Environ Sci Technol, **45** (7), 2909, **2011**.
45. MCKNIGHT D., BOYER E., WESTERHOFF P., DORAN P., KULBE T., ANDERSEN D. Spectrofluorometric Characterization of Dissolved Organic Matter for Indication of Precursor Organic Material and Aromaticity. Limnology and Oceanography, **46**, 38, **2001**.
46. CHEN Z.Y., LI S.Y. Absorption and Fluorescence Spectra of Dissolved Organic Matter in Rivers of the Three Gorges Reservoir Area Under the Background of Urbanization. Environ. Sci. **40**, 5309, **2019**.
47. ZHANG R., LIU Z., XIONG, K., LYU X., HU C., WANG X., CHENG K. Analysis of the Three-Dimensional Fluorescence Spectroscopy Characteristics of Dissolved Organic Matter in Groundwater from a Subtropical Cave in Dry Season – Daxiao Cave in South China Karst. Water, **24** (13), 3574, **202**1.
48. HUGUET A., VACHER L., RELEXANS S., SAUBUSSE S., FROIDEFOND J.M., PARLANTI E. Properties of fluorescent dissolved organic matter in the Gironde Estuary. Organic Geochemistry, **40** (6), 706, **2009**.
49. KIDA M., TANABE M., TOMOTSUNE M., YOSHITAKE S., KINJO K., OHTSUKA T., FUJITAKE N. Changes in dissolved organic matter composition and dynamics in a subtropical mangrove river driven by rainfall. Estuarine, Coastal and Shelf Science, **223**, 6, **2019**.
50. SINGH S., D'SA E.J., SWENSON E.M. Chromophoric dissolved organic matter (CDOM) variability in Barataria Basin using excitation-emission matrix (EEM) fluorescence and parallel factor analysis (PARAFAC). Science of The Total Environment, **408** (16), 3211, **2010**.
51. JIANG T., WANG D., MENG B., CHI J., LAUDON H., LIU J. The concentrations and characteristics of dissolved organic matter in high-latitude lakes determine its ambient reducing capacity. Water Research, **169**, 115217, **2020**.
52. KULKARNI H.V., MLADENOV N., MCKNIGHT D.M., ZHANG Y., KIRK M.F., NEMERGUT D.R. Dissolved fulvic acids from a high arsenic aquifer shuttle electrons to enhance microbial iron reduction. Science of The Total Environment, **615**, 1390, **2018**.